Supplement of Biogeosciences, 21, 1433–1459, 2024
https://doi.org/10.5194/bg-21-1433-2024-supplement

Biogeosciences Open Access EGU

Supplement of

Oceanographic processes driving low-oxygen conditions inside Patagonian fjords

Pamela Linford et al.

Correspondence to: Iván Pérez-Santos (ivan.perez@ulagos.cl)

Configuration and validation Hydrodynamics Model

To ensure the accuracy and reliability of the MIKE 3 FM hydrodynamic model, validation processes were undertaken. This supplementary material delves into the specific configuration and validation methodologies employed and contrasts the model results with observational datasets.

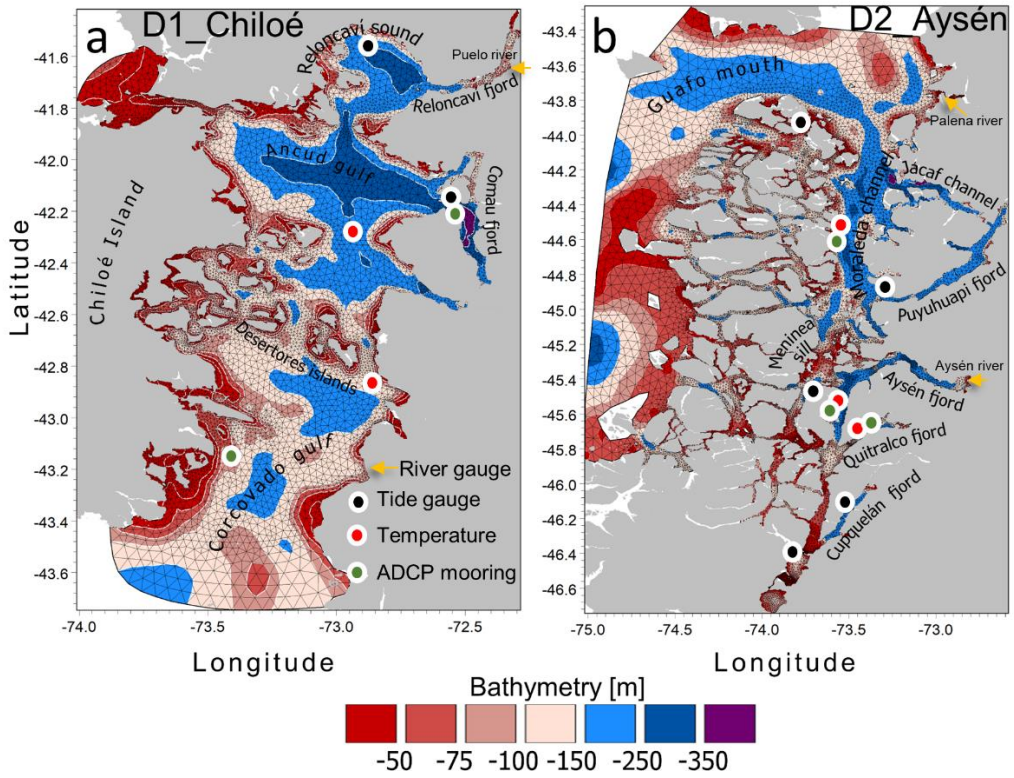

Figure S1: High-resolution model domain includes the northern Patagonia inner sea and is denoted as D1_Chiloé, while D2_Aysén covers the southern section. Bathymetry used was based on SHOA nautical chart from the Chilean Navy. For validation purposes, various measurement locations are marked: black dots represent tide gauge stations, red dots indicate the placements of temperature sensor moorings, green dots denote the locations of ADCP moorings and yellow arrow represent river gauge.

The use of two overlapping domains, D1_Chiloe and D2_Aysen (Fig. S1) was influenced by computational capacity, resulting in a staggered development over time, from 2016 onwards. The D1_Chiloe domain was developed first, followed by the D2_Aysen domain. The model included 55 layers for D1_Chiloe and 40 layers for D2_Aysen, which were utilized to accurately depict stratification, focusing on the highest resolution in the upper water column (approximating ~ 1m near the surface). Horizontal eddy viscosity was characterized using the Smagorinsky model (Smagorinsky, 1963), while the vertical eddy viscosity was incorporated through the $\kappa - \varepsilon$ turbulence scheme, which solves the transport equations for both turbulent kinetic energy (κ) and turbulent dissipation rate (ε) (Rodi, 1984). Bathymetry was based on SHOA nautical chart soundings, and a digital elevation model was constructed using the natural neighbor method (Sibson, 1981). This domain was discretized using triangular elements of different sizes. The

highest resolution was observed in coastal, narrow, and shallow areas, with an average element size of ~300 m, whereas the spatial resolution near the boundary was ~1000 m.

Table S1. Detail of instruments used for the hydrodynamic model validation.

	Instrument (Source)	Geographics Coordinates		Time frame validation
Puerto Montt	Tide gauge (SHOA)	-72.96, -41.48		01/01/2017 31/12/2017
Comau	Tide gauge (IFOP)	-72.42	-42.38	30/10/2020 26/09/2021
Melinka	Tide gauge (IFOP)	-73.73	-43.90	15/07/2017 28/03/2018
Puyuhuapi	Tide gauge (IFOP)	-73.30	-44.90	08/06/2018 13/03/2019
Errazuriz	Tide gauge (IFOP)	-73.77	-45.46	10/06/2018 15/03/2019
Elefante	Tide gauge (IFOP)	-73.74	-46.40	16/08/2018 06/03/2019
Cupquelán	Tide gauge (IFOP)	-73.44	-46.12	17/08/2016 08/03/2017
Puelo River	Flow gauging station (DGA)	-72.24	-41.61	01/01/2016 30/12/2018
Palena River	Flow gauging station (DGA)	-72.44	-43.96	01/01/2016 30/12/2018
Aysén River	Flow gauging station (DGA)	-72.72	-45.40	01/01/2016 30/12/2018
Mouth Comau Fjord	ADCP RDI-300 kHz (IFOP)	-72.50	-42.19	09/11/2020 23/09/2021
Corcovado	ADCP RDI-300 kHz (IFOP)	-73.41	-43.10	12/12/2019 08/02/2020
Moraleda Channel	ADCP RDI-300 kHz (IFOP)	-73.50	-44.63	21/08/2018 10/03/2019
Costa Channel	ADCP RDI-300 kHz (IFOP)	-73.51	-45.47	24/08/2018 08/11/2018
Quitralco Fjord	ADCP RDI-300 kHz (IFOP)	-73.45	-45.74	17/03/2019 10/10/2019
Ayacara Pass	Temperature sensor (IFOP)	-72.92	-42.31	08/07/2017 22/03/2018
Desertores Pass	Temperature sensor (IFOP)	-72.87	-42.78	07/07/2017 23/03/2018
Moraleda Channel	Temperature sensor (IFOP)	-73.50	-44.63	08/08/2018 10/03/2019
Costa Channel	Temperature sensor (IFOP)	-73.51	-45.47	23/08/2018 15/03/2019
Quitralco Fjord	Temperature sensor (IFOP)	-73.45	-45.74	25/08/2018 17/3/2019

DGA, Chilean Water Authority (www.DGA.cl). IFOP, Instituto de Fomento Pesquero (www.IFOP.cl). SHOA, Hydrographic and Oceanographic Service of the Chilean Navy (www.SHOA.cl)

Atmospheric forcings, such as wind stress and heat fluxes over the sea surface, were introduced using spatially and temporally varying fields from the Weather Research and Forecasting (WRF) atmospheric model (Skamarock et al., 2008). The performance of the WRF-IFOP model was evaluated as described by Pinilla et al. (2020). Soto-Riquelme et al. (2023) evaluated the performance of the WRF-IFOP model near the Guafo Mouth and confirmed its effective correlation with meteorological stations in at area. Their results revealed a high correlation with atmospheric pressure (R=0.99), accompanied by significant correlations for wind direction: R=0.81 for the east-west component and a more robust correlation of R=0.94 for the north-south component (Soto-Riquelme et al., 2023).

Freshwater sources were identified through the FLOW-IFOP hydrological model, which employs precipitation and temperature series data from the CR2MET gridded product (http://www.cr2.cl/datos-productos-grillados/). Using this data, characterized by a spatial resolution of 5 × 5 km, enables the simulation of runoff and the calculation of daily discharge series. The performance of the FLOW-IFOP model at the gauged river stations of the Chilean Water Authority can be accessed at http://chonos.ifop.cl/flow/. Furthermore, the correlations for the three main rivers in these regions—Puelo, Palena, and Aysén, Table S1, Fig. S1 were found to be 0.88, 0.76, and 0.87 respectively (see Fig. S2 in the supplementary material).

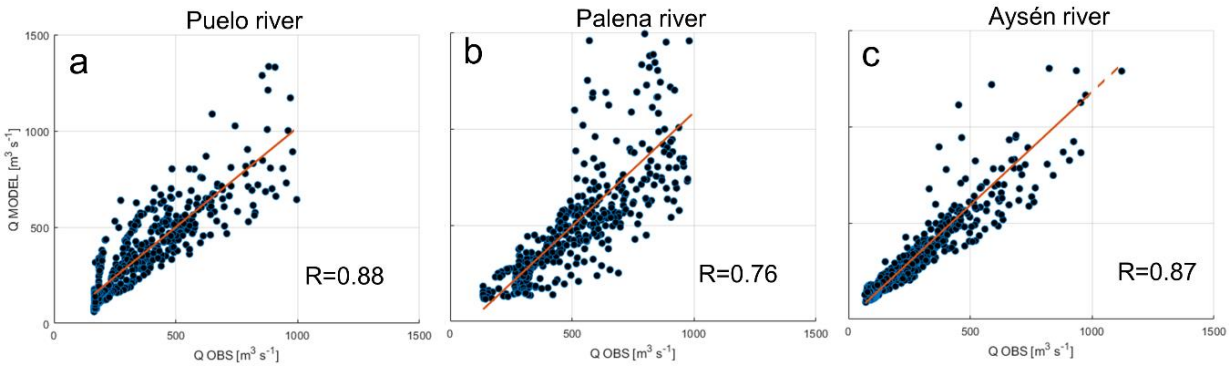

Figure S2. Relationship between observed and modeled data of the main rivers discharge. Data from the Chilean Water Authority and the FLOW-IFOP model corresponding to a) Puelo River, b) Palena River, and c) Aysén River. The correlation coefficient indicates the strength of the correlation between the observed and modeled data.

Table S2: Comparison of amplitude and phase of the semidiurnal M2 and diurnal K1 tidal harmonic components at different locations. The results demonstrate robust correlations between the sea level at different stations, with correlations ranging from 0.93 to 0.97.

Site	Tide Gauge	Model	Tide Gauge	Model	Tide Gauge	Model	Tide Gauge	Model	R Amplitude
	M2 Amplitude		K1 Amplitude		M2 Phase		K1Phase		
Puerto Montt	1.86	2.11	0.26	0.23	169	159.1	66.9	71.56	0.97
Comau	1.84	1.9	0.23	0.28	158	342	60	7.93	0.96
Melinka	0.72	0.64	0.18	0.24	141	152	79	67.3	0.95
Puyuhuapi	0.79	0.7	0.19	0.25	149	161	71	69	0.96
Errazuriz	0.71	0.69	0.19	0.25	152	171.32	72	73.41	0.93
Elefante	1.09	1.02	0.21	0.27	190	198.2	83	84.41	0.97
Cupquelán	1.1	1	0.21	0.27	189	198.9	82	85.7	0.97

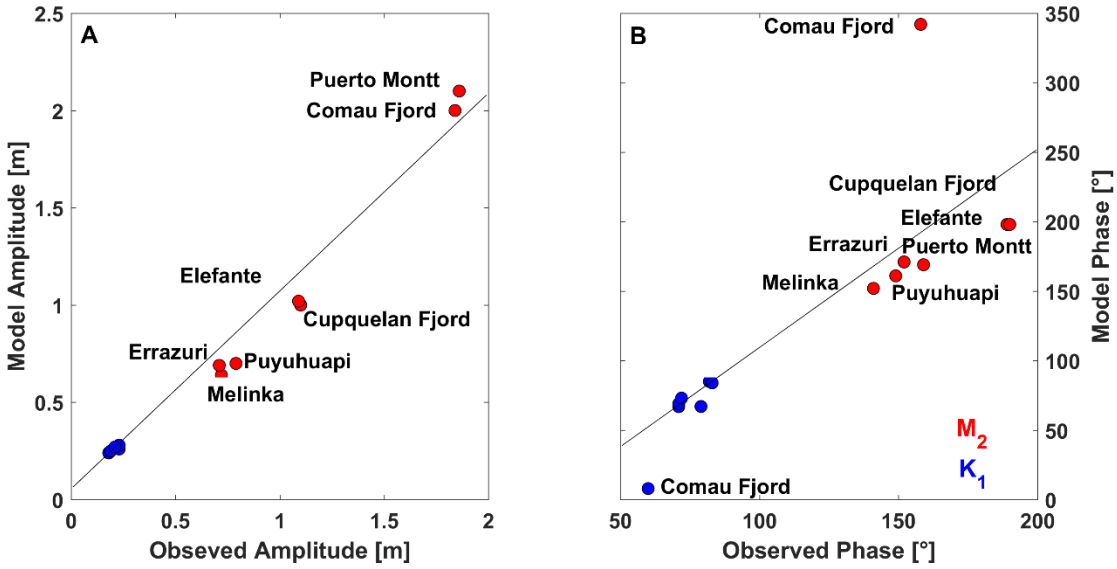

Figure S3. Modeled and observed (a) amplitude and (b) phase for M2 (red) and K1 (blue) tidal harmonics. They exhibited an appropriate amplification of amplitude particularly in the northern area of this domain (Puerto Montt and Comau fjord) (Figure S3).

The performance of the current data within the models contrasted with the ADCP data from different mooring points (Figure S1, Table S1). The hydrodynamic model current was evaluated against the current velocities gathered by the ADCP. An empirical orthogonal function analysis (Thomson and Emery, 2014) was performed on the currents (both observed and modeled) to discern if the model could accurately depict the dominant modes of variability

identified with the observations. Similar analyses have been previously performed to assess the suitability of hydrodynamic models in Patagonia (Pinilla et al., 2020, Soto-Riquelme et al., 2023).

Mode 1 and Mode 2 accounted for over 95% of the variance in the model, whereas they represented approximately 86% in the observations, except in the Quitralco fjord, with a 77% variance observed in the model and 62% in the ADCP (Figure S4). The distribution of these percentages of variance between the model and the ADCP was correlated with an R-value of 0.96, as shown in Figure S5, highlighting the distinctiveness of the Quitralco fjord. On the other hand, the spatial vertical structures of Modes 1 and 2 between the model and the ADCP data were congruent, generally showing alignment in barotropic structures, two-layer baroclinic structures, and even three-layer structures, as observed in the Quitralco fjord (Figure S4). While the model is not without limitations, our analysis suggests a congruence between the modes of variability, further implying the proficiency of the model in representing the primary processes of water transport in various locations.

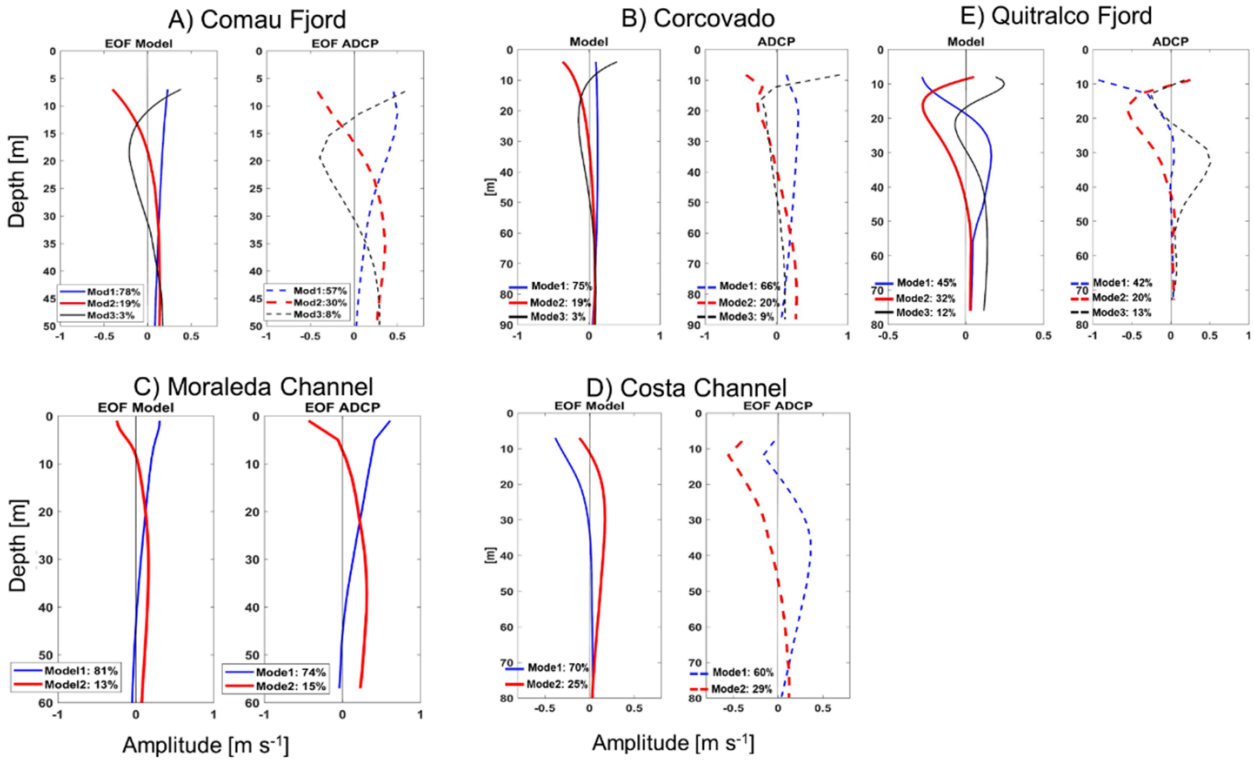

Figure S4. Empirical Orthogonal Function (EOF) analysis of the main component of current velocities at a) Comau Fjord, b) Corcovado Gulf, c) Moraleda Channel, d) Costa Channel, and e) Quitralco Fjord. Left-side graphs display the model output, while right-side graphs show the corresponding ADCP measurements. The legends indicate the percentage of explained variance for each mode.

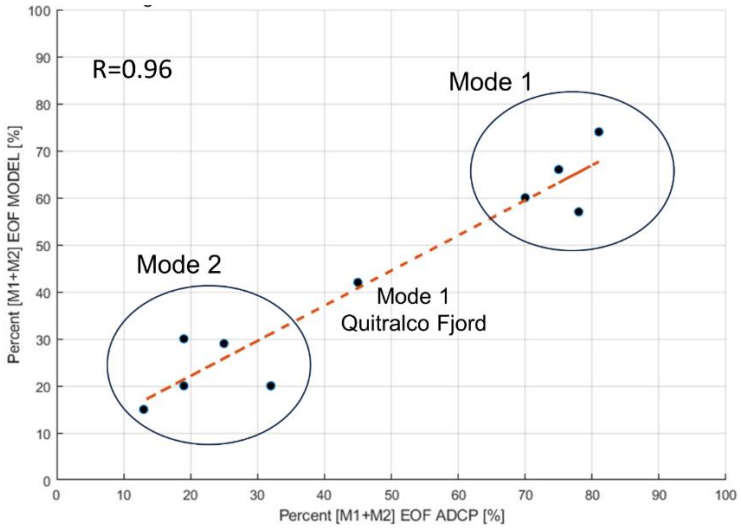

Figure S5. Percentage contribution of mode 1 and mode 2 in both the model and ADCP data. The correlation coefficient between the model and ADCP contributions is provided.

The performance of temperature time series demonstrated commendable alignment in replicating the annual temperature cycle at various depths and locations (Table S1, Figure S1), generally exhibiting R-values above 0.78. An exception was observed in the Moraleda Channel at a depth of 120 m, where a lower R-value (0.28) was recorded (Figures S6 and S7).

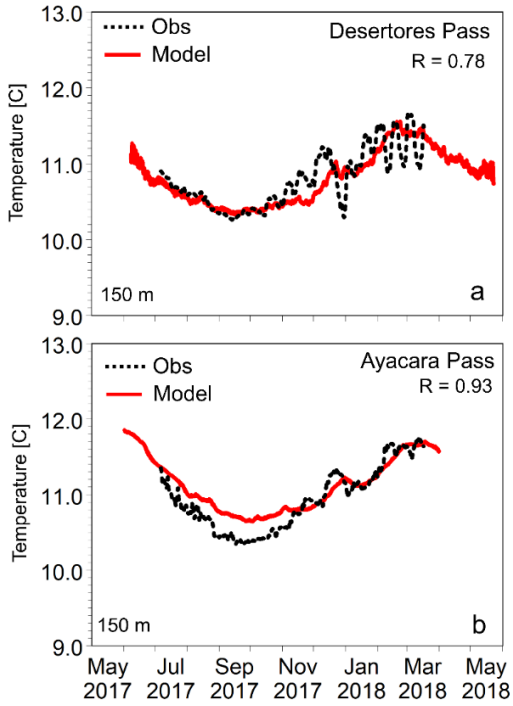

Figure S6. Time series of temperature at 150-m depth at a) Desertores Pass and b) Ayacara Pass. Observed data is shown in black and modeled data is shown in red; their correlation coefficient is provided.

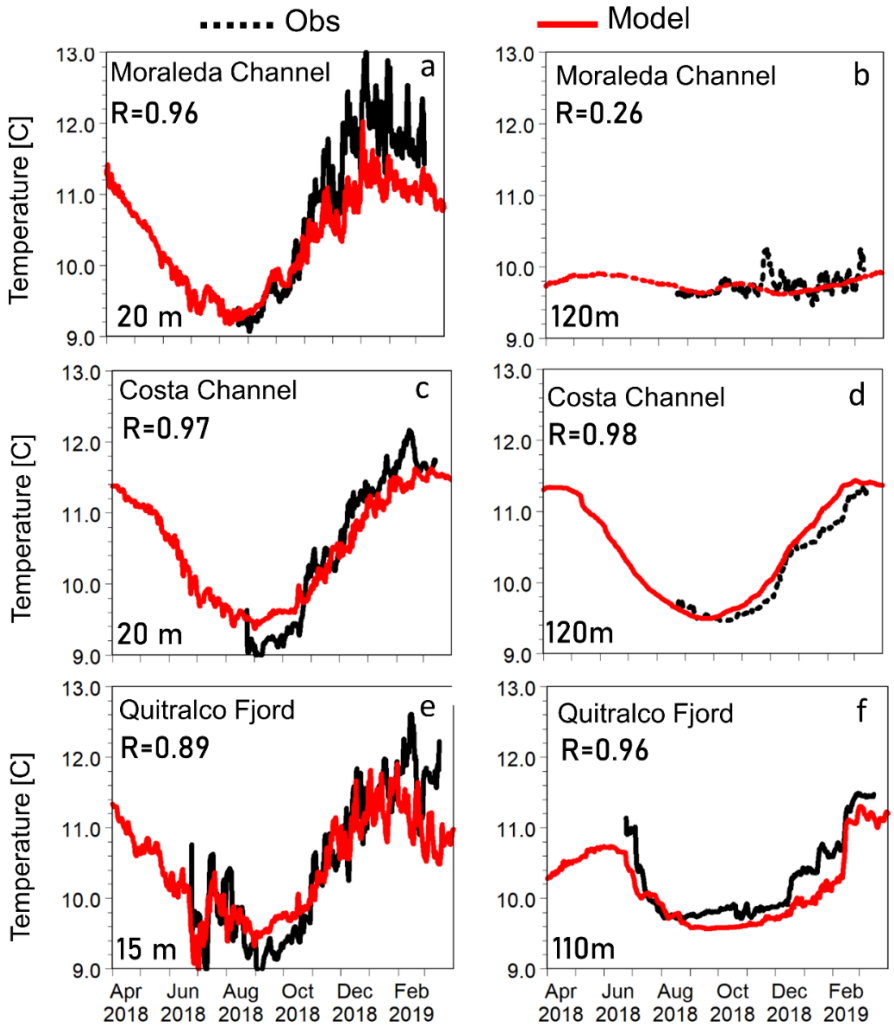

Figure S7. Time series of temperature at (a) 20 m and (b) 120 m in Moraleda Channel, (c) 20 m and (d) 120 m in Costa Channel, and (e) 15 m and (f) 110 m in Quitralco Fjord. Observed data is shown in black and modeled data is shown in red; their correlation coefficient is provided.

To assess the water masses present within the fjords, salinity was employed as a key parameter. High salinity waters (>33.5 g kg^{-1}), associated with SAAW and ESSW ocean masses, enter the deep layer of the Guafo mouth, traverse the Corcovado Gulf, and end their journey in the deep layers of the Puyuhuapi Fjord and Jacaf Channel. A reduction in salinity, indicative of Estuarine Water (EW), is also observed due to the melting of ice from the San Rafael Lagoon. The model's task was to accurately depict the arrival of specific salinity categories inside the fjords and channels (see Figure S8 in the Supplementary Material). Although the 34 g kg^{-1} isohaline is not visually present within the model domains, we believe the model successfully replicates the spatial structure, which suggests that the processes controlling salinity transport within the fjords were successfully incorporated. While the model may not perfectly replicate these processes, it does allow us to understand the fundamental physical transport mechanisms at play.

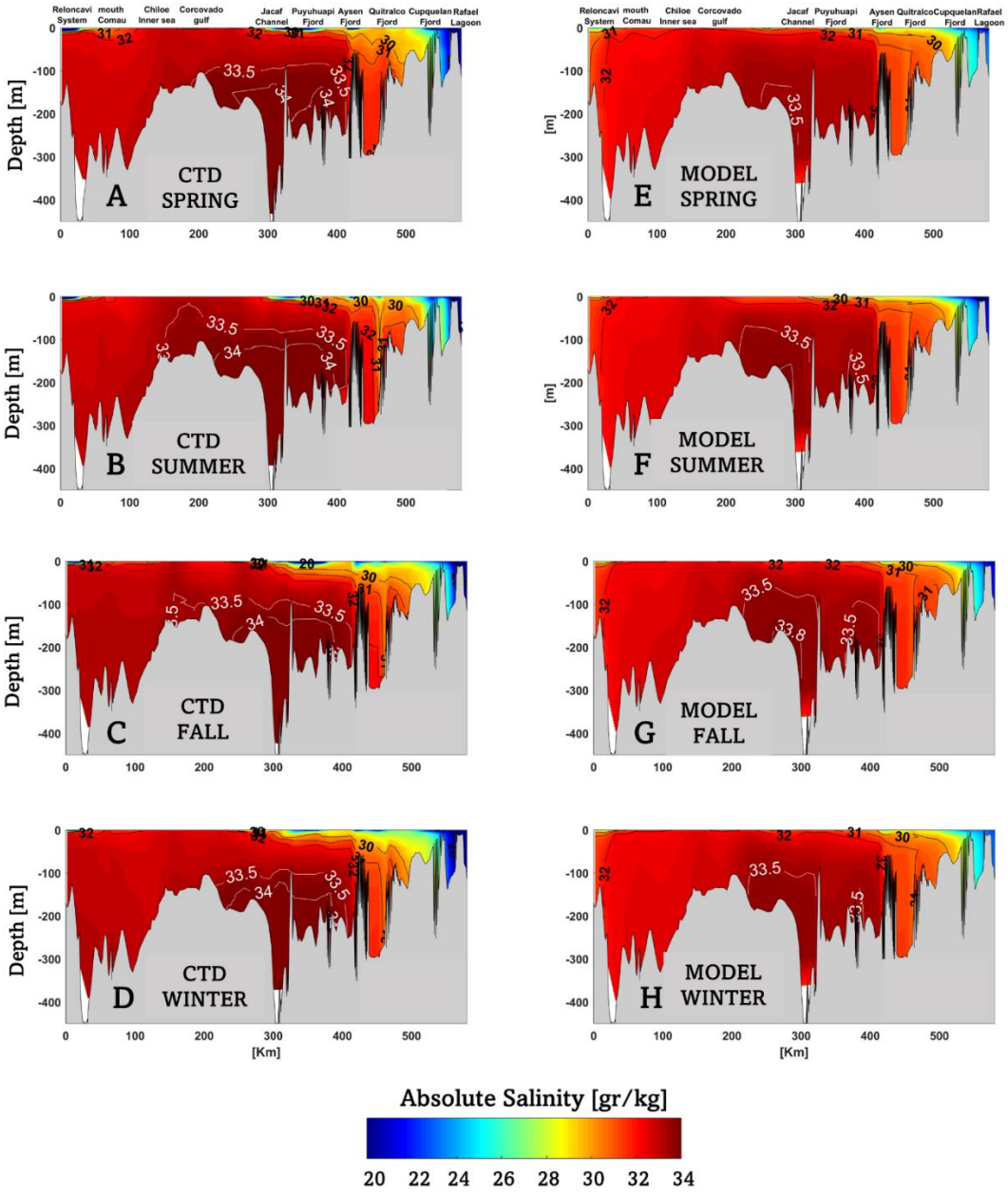

Figure S8. Absolute salinity (g/kg) along northern region of Patagonian fjords for CTD Stations (A, B, C, D) during oceanographic expeditions (2020 to 2021) and seasonal mean (2020–2021) for hydrodynamic model (E, F, G, H). Left panel (CTD) and right panel (model) showed good agreement, higher salinity (>33 gr/kg) associated with SAAW and ESSW ocean waters, entering the deep layer of the Guafo mouth, crossings the Corcovado Gulf, and ends its travel at the deep layers of the Puyuhuapi Fjord and Jacaf Channel. A decrease in salinity due to ice melting from the San Rafael Lagoon is also seen, which indicates the presence of estuary water (EW).

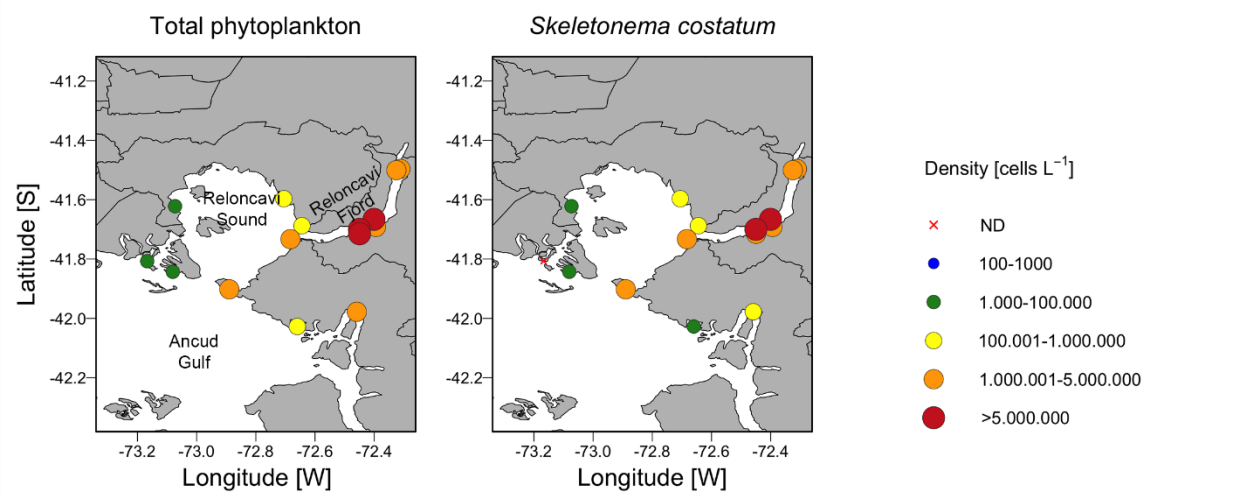

Figure S9. *In-situ* phytoplankton sampling in the Reloncaví Fjord and Reloncaví Sound showing the abundance of *Skeletonema costatum* during May 2017.